Electronic Supplementary Information

ESI-1: Data Processing

The data processing algorithm developed is complex and consists of many steps, and the necessity for a simplified explanation quickly became apparent. To this end, we have divided the algorithm into three data processing stages: a) pre-processing, b) main processing, and c) post-processing. The following explains each stage in detail:

a) Data Pre-processing Stage

The aim of the pre-processing stage is two-fold: 1) provide a NP detection threshold and 2) separate the metal NP signal from the ionic metal signal. The NP detection threshold is obtained by subjecting the raw, time-resolved data from a single line scan to median filtering. Median filtering is commonly used for the removal of noise in digital image processing; however, in LA-sp-ICPMS, many of the observed "spikes" in the time-resolved signal originate from NPs. Median filtering produces essentially the ionic metal signal (insomuch as is possible to separate the metal ionic signal from the very small metal NPs, below the NP sizing limit). After median filtering, for each resulting data point (now the median, μ, of the raw signal), the Poisson noise is calculated:

$$\sigma = \sqrt{\mu} \quad (1)$$

To ensure the absence of false positive NP detections, we use a 5σ threshold criterion[1]. Thus, the resulting local NP detection threshold T_{loc} at each data point is:

$$T_{loc} = \mu + 5\sigma \quad (2)$$

Derived this way, the NP detection threshold T_{loc} gives a level of zero for parts of the line scan where the ionic metal concentration is low and NPs are absent. This can result in the false detection of background noise as NP peaks. To avoid this, a user-defined artificial threshold, T_{art}, is used, replacing all zero values of T_{loc}, resulting in the final NP detection threshold T_{det}.

In parallel, the median filtered data is smoothed with Gaussian kernel filtering and subtracted from the raw data. Data points above the smoothed median filter are considered to be associated with the NP signal (for the purpose of individual peak integration), and the remaining data points are related to the ionic metal signal.

Figure S1 shows how the pre-processing stage generates three data sets: 1) the ionic metal signal, 2) the NP detection threshold for identifying the peaks and 3) the NP signal used for peak integration.

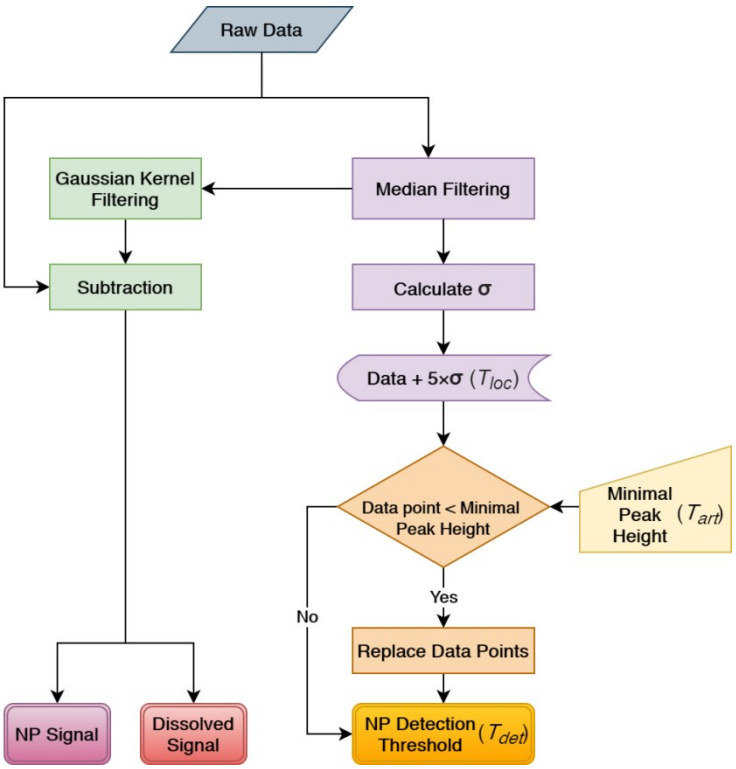

Figure S1. Pre-processing stage.

b) Main Processing Stage

After the metal NP signal has been separated from the ionic metal signal in the pre-processing stage, it is subjected to NP peak identification, followed by peak integration via summation of data points in each peak. At this point, one of the intrinsic challenges of LA-sp-ICPMS presents itself, *viz.*, how to deal with overlapping peaks? In solution sp-ICPMS, when the NP number concentration is too high and there is a considerable risk of overlapping NP peaks, the obvious solution is to dilute the sample. However, in LA-sp-ICPMS one can reduce the beam size *BS* and/or repetition rate *RR*, assuming that the system response time (associated with the dispersion of NPs in the LA cell and interface) is not faster than say 0.5 s. Given that in biological matrices the NP number concentration varies with location, the likelihood of overlapping NP peaks differs from location to location. For this reason, the dataset containing the NP peak positions found is used to determine the positions of peaks which are separated by more than 200 µs and less than 600 µs. Those peaks, classified as overlapping peaks, are deconvolved by a peak fitting algorithm developed by O'Haver[2]. The newly deconvolved peak areas are then used instead of the original integrated values. **Figure S2** shows the steps involved in this main processing stage, resulting in the generation of NP peak positions and their intensities (in counts) for each line scan.

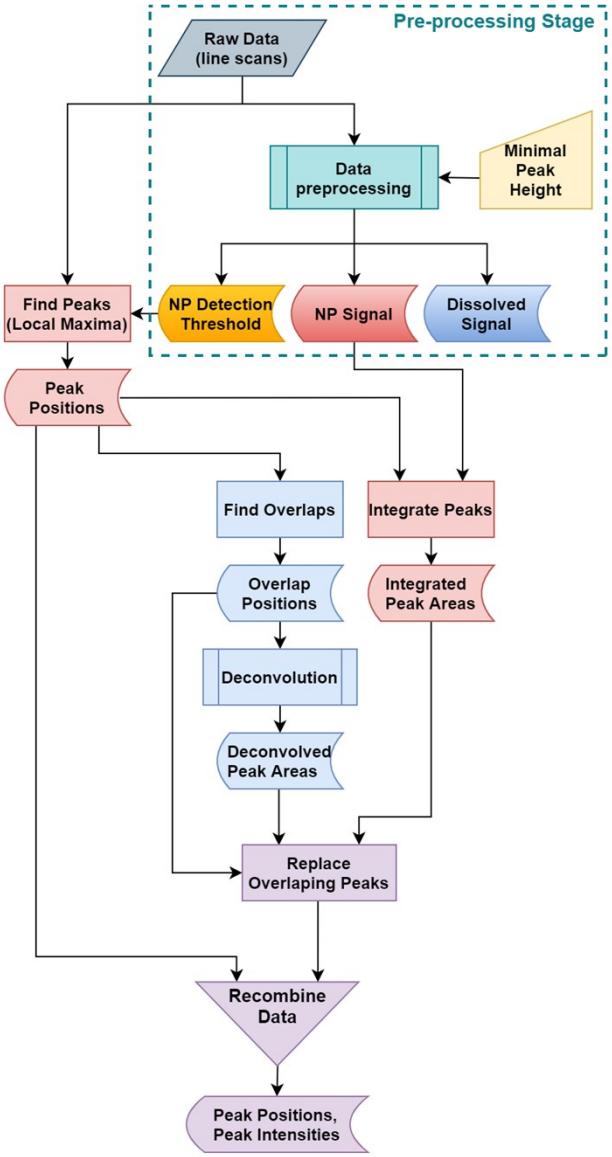

Figure S2. Main processing stage.

c) Post-processing Stage

The final data processing stage mainly deals with reorganizing the processed data into maps and outputting the data in an appropriate format for display. In post-processing, the NP peak intensities, Ct_{NP} (in counts), are converted to NP size, S_{NP} (in nm), using a sizing standard, *i.e.*, a gelatin standard containing well-characterized NPs of known size, $S_{NP,std}$, and determining their mean integrated area, $Ct_{NP,std}$, in counts. Assuming that the detected NPs are spherical, the size of each particle is calculated by

$$S_{NP} = \sqrt[3]{Ct_{NP}} * \frac{S_{NP,std}}{\sqrt[3]{Ct_{NP,std}}} \qquad (3)$$

After conversion of NP peak intensity to NP size, the resulting data is segregated by NP size in steps of 10 nm (or in custom size range intervals using the online LA-sp-ICPMS Mapping Analysis App as explained in **ESI-2**). Following size segregation, all of the line scan-processed data is converted into maps by simple matrix reshaping based on the number of lateral pixels. The columns of the reshaped matrices for the ionic metal signal and unprocessed signal are summed to obtain the ionic metal map and the total metal content map, respectively. The total metal NP count map and size segregated metal NP maps are obtained similarly, only instead of summing the columns, the NP occurrence is counted and the NP counts per pixel are reported. Segregating the NPs by size into separate maps allows for simultaneous visual assessment of NP size distribution and their spatial distribution. It is worth emphasizing that the total metal content and ionic metal content maps directly display the measured signal intensity per pixel, whereas the NP maps show the number of particles detected per pixel, whether total or size segregated. **Figure S3** summarizes the steps involved in the visualization of the data.

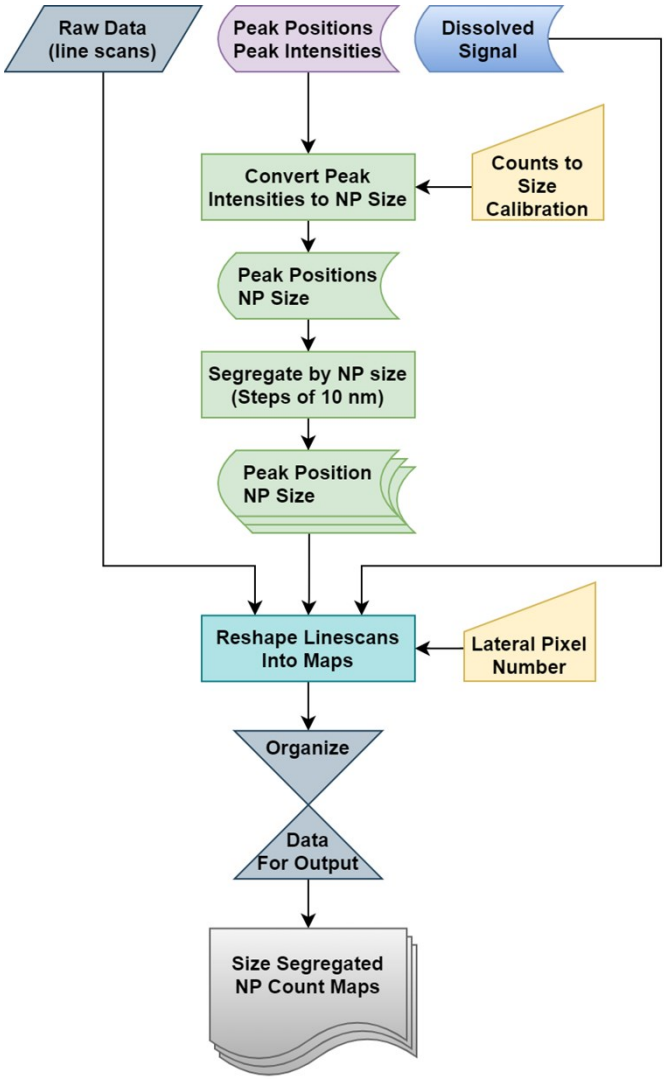

Figure S3. Post-processing stage.

ESI-2: Online App for Data Visualization

To get insight into the distribution of AgNPs in root cross-sections of sunflower plants exposed to 1, 4 and 40 µg g^{-1} $AgNO_3$ in hydroponics, an online LA-sp-ICPMS Mapping Analysis App (https://laicpms-apps.ki.si/webapps/home/) is available that allows users to freely select a region (square, circle or freehand) on the AgNP maps obtained in this work, followed by automatically computing and the AgNP : Ag^+ mass ratio in that region and displaying the AgNP frequency distribution in a histogram (the app also provides for displaying of the AgNP maps in a custom size range).

Online App User Instructions

In the online app, 17 samples measured by LA-sp-ICPMS and the processed data are available for visualization and analysis. Upon starting the app, the user must first select a data set for a sample from a drop down menu (1) and load it by pressing the “Load Sample” button (2).

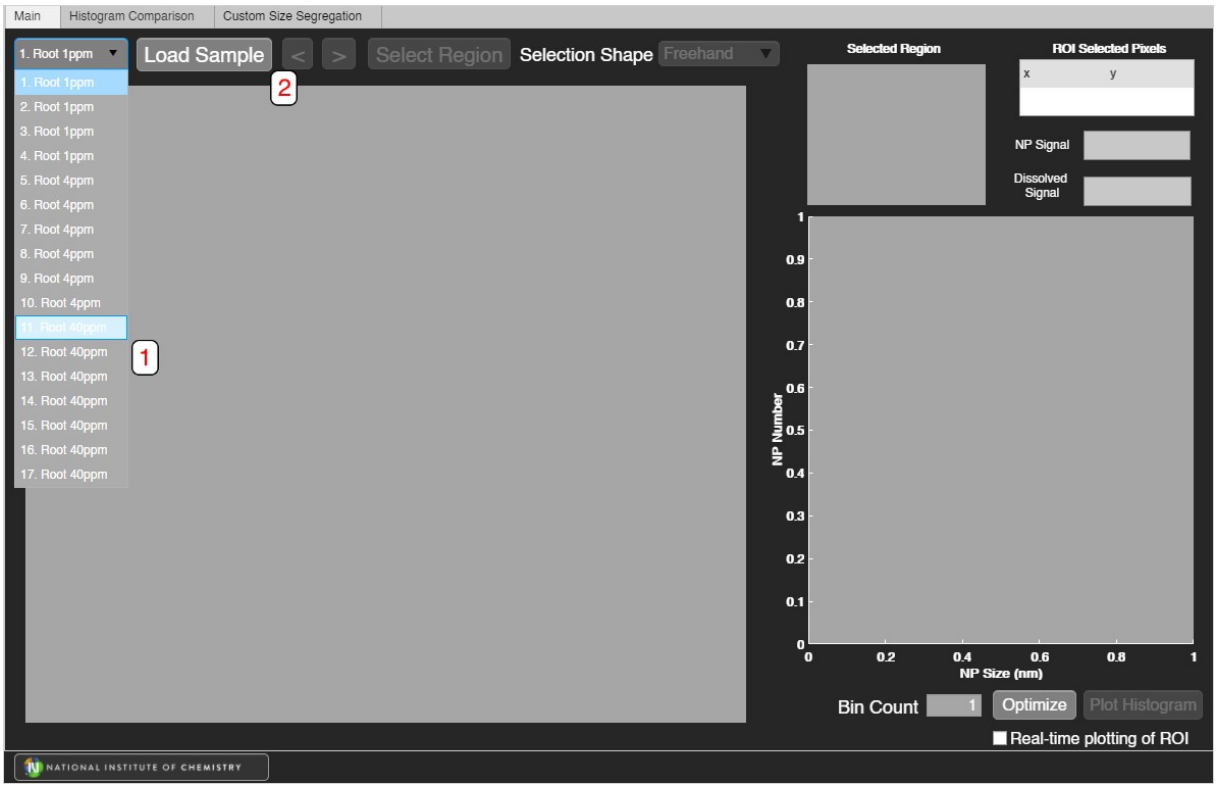

After the sample data has finished loading, it is possible to change the displayed size range, in steps of 10 nm, by clicking the “<” and “>” buttons (3). Clicking on the “Select Region” button (4) allows the selection of a region of interest (Circular, Rectangular or Freehand). Upon selecting a region of interest in the NP map (5), pressing the “Plot Histogram” button (6) will create a NP size histogram associated with the selected region.

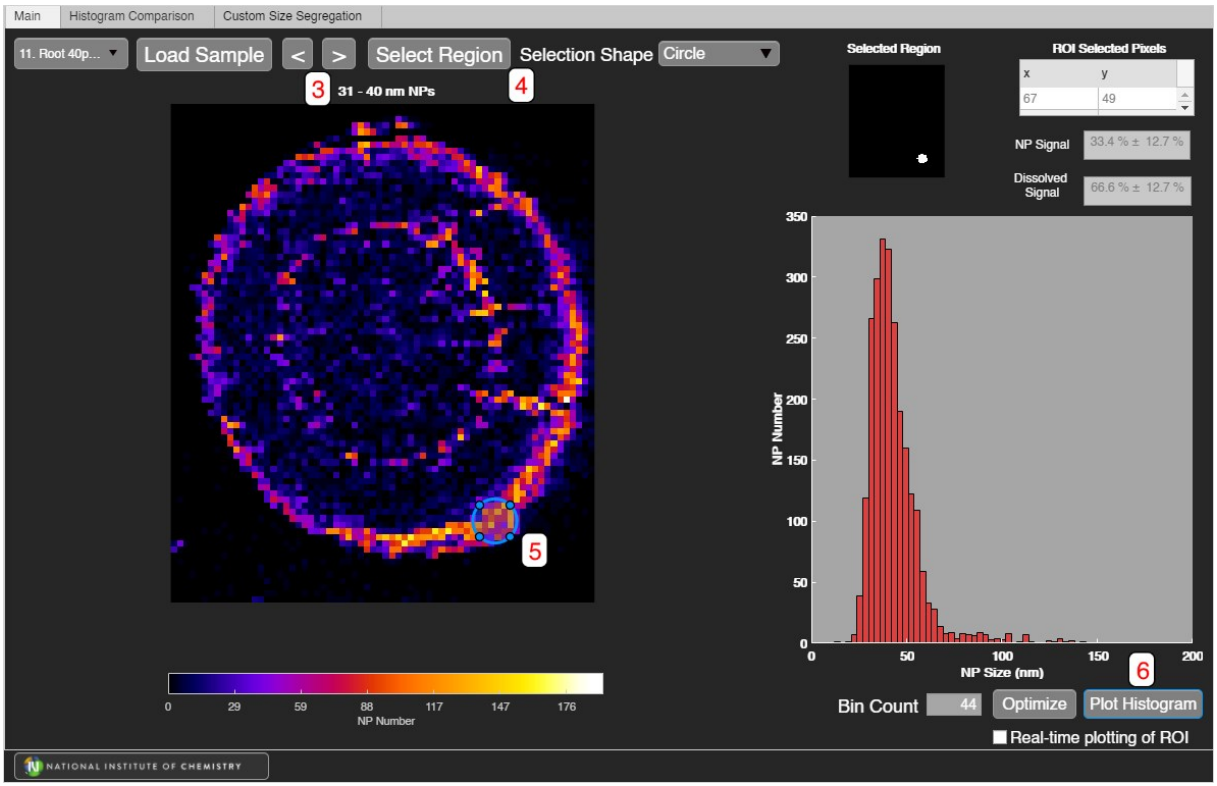

After plotting the selected region of interest NP size histogram, under the “Histogram Comparison” tab, it is possible to compare multiple NP size histograms. The “Store” button (7) saves the currently displayed histogram from the “Main” tab. The user is then free to select another region of interest and create a second histogram. After two or three histograms have been saved, they can be compared by pressing the “Combine” button (8). This superimposes the saved histograms for easier comparison.

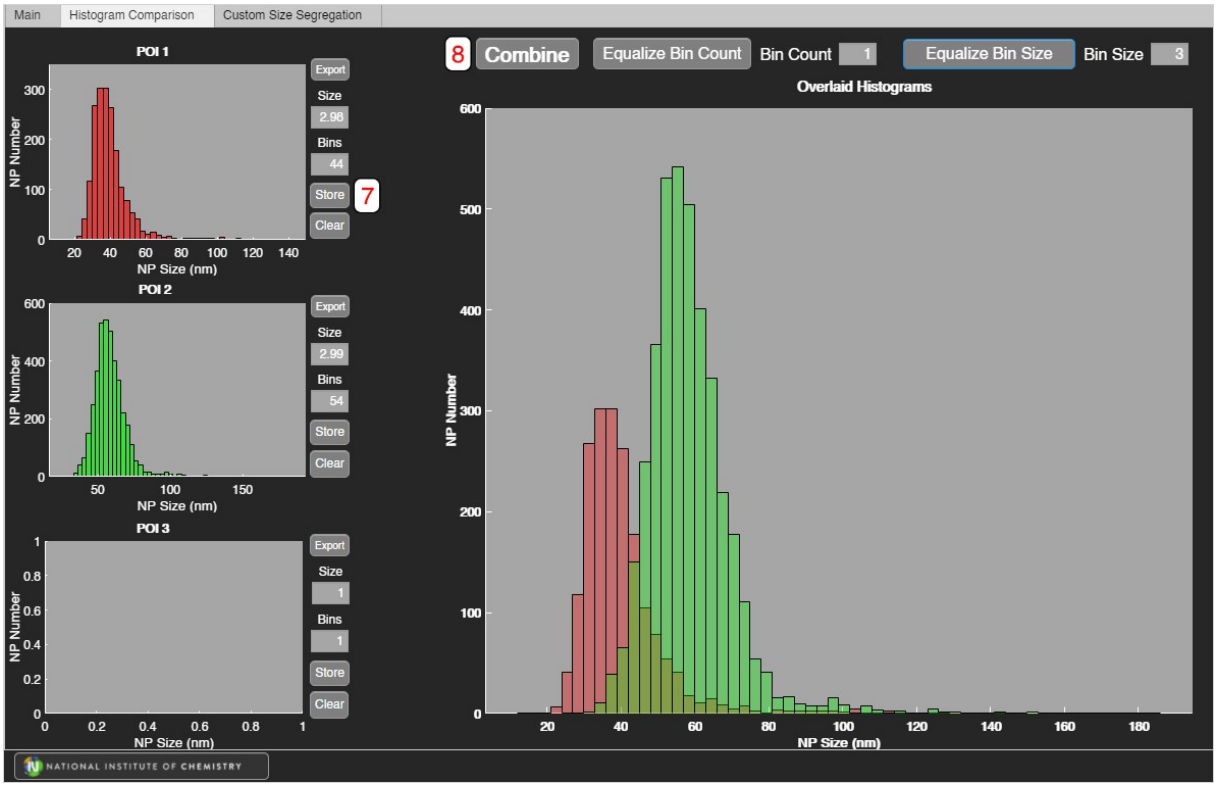

The app also allows for the creation of custom size range maps from the processed sample data. On the “Custom Size Segregation” tab, a custom size range can be selected by typing in the NP spherical size equivalent (9). Pressing the “Get Image” button creates a NP number map for the selected size range.

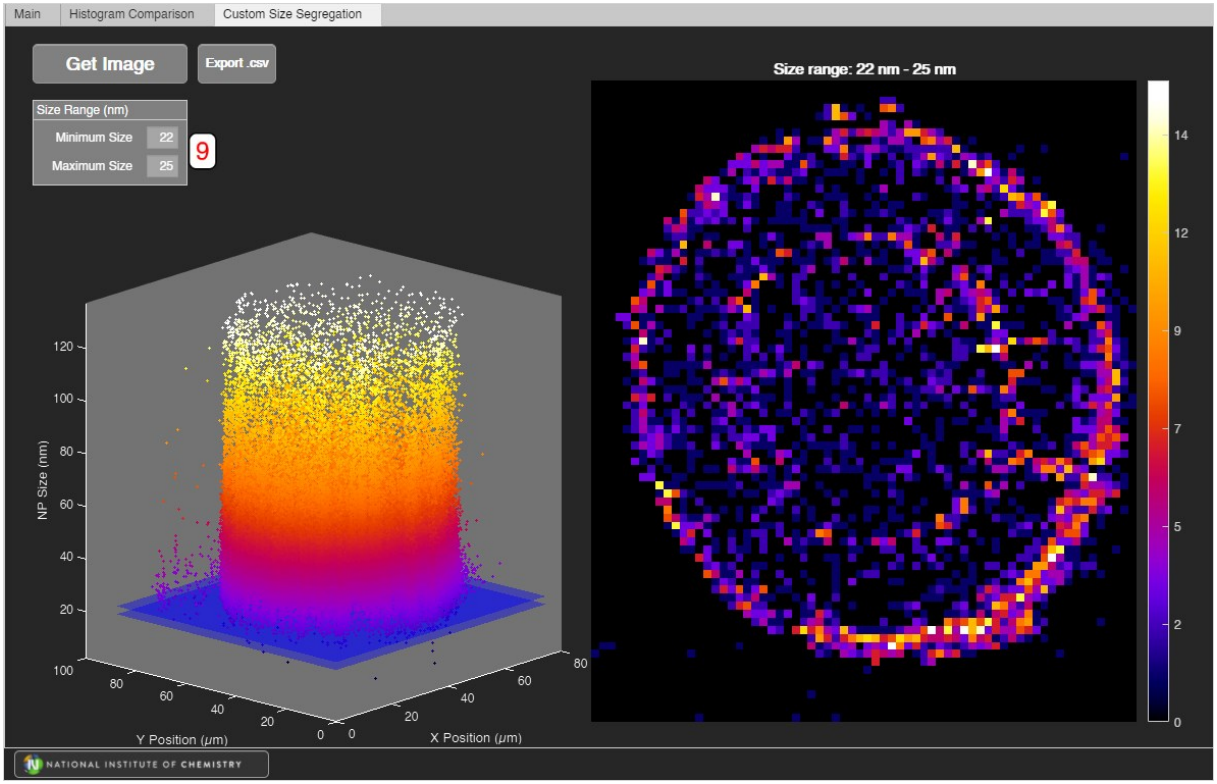

ESI-3: Concise Overview of Ionic Silver Uptake in Plants

The uptake of ionic silver (Ag^+) in plants is a multifaceted problem involving many different processes occurring in parallel. A large number of membrane proteins are involved in the transport and oxidation/reduction of metal ions from the environment.

Ag^+ uptake is intrinsically linked to the uptake of copper and to a certain extent, metal uptake in general. Plants can use two strategies to uptake metal ions, *viz*., chelating (I) and reductive (II) strategies[3].

Strategy I involves the release of chelating compounds by the plant which subsequently bind to the metal ions and are subsequently transported as metal-ligand complexes into the cells by transporter proteins present in the cell membrane. While strategy I is not directly related to copper and silver uptake, it is relevant since some of the chelating agents released do show reductive properties which, taking into consideration the standard reduction potential of Ag^+/Ag^0 of 0.8 V, can cause reduction of Ag^+ in the cell wall.

Strategy II involves the reduction of metal species by enzymes present in the cell membrane, followed by the uptake of their reduced form by membrane transporters.

Copper is an essential element in eukaryotic cells and is present in many of its enzymes.[4] Depending on the environmental conditions, copper can be present in both Cu^{2+} and Cu^+ form. Cu^{2+} is reduced to Cu^+ by the plasma membrane NADPH-dependent ferric reductase oxidases (FRO), and then transported into the cell by the copper transporter protein (Ctr/COPT)[5].

After entering the cell, Cu^+ plays a critical part in at least three different pathways by binding to metallochaperones (small proteins that bind Cu^+)[6]. In this way, the concentration of free copper (Cu^{2+} and Cu^+) inside the cells is kept very low, and the metallochaperone-bound Cu^+ is shuttled to the required site of action. The three different pathways include:

1. shuttling of Cu^+ to the cytosolic radical scavenging enzyme SOD1 (superoxide dismutase 1), which is carried out by CCS (copper chaperone for superoxide dismutase);
2. shuttling of Cu^+ to P-type ATPases, which then incorporate the metal into cuproproteins in the trans-Golgi network and/or vesicles of the secretory pathway, which is carried out by ATX1 (antioxidant protein 1) and CCH (copper chaperone);
3. the use of copper for the metalation of CCO (cytochrome *c* oxidase) in the mitochondria.

The exact fate of copper immediately after entering the cytosol is uncertain. There is evidence that Cu^+ is sequestered by cytoplasmic metallochaperones for transport to specific organelles and copper proteins; however, it is unclear whether the chaperones interact directly with the Ctr/COPT or that an intermediate Cu^+ carrier is involved. Glutathione may serve the role of a copper transporter in the absence of metallochaperones, as down-regulation of metallochaperones was shown to have little effect on the copper uptake.[7,8]

After Ag^+ has entered the cytosol and is bound to metallochaperones, and other metal concentrations in the cytosol exceed a certain level, the metal binding capacity of metallochaperones and organic molecules can be overloaded. In this case, cysteine-rich proteins called metallothioneins, which have a high affinity for Cu, Zn, Cd and Ag, can buffer the excessive metal levels[3]. To increase their metal binding capacity, plants will synthesise oligomers of glutathione with the enzyme phytochelatin synthase. Phytochelatin (PC) is a 2-10 unit oligomer of glutathione that can bind Cu, Zn, Cd and Ag. Excess PC-metal complexes can be stored in vacuoles after being transported by ATP-binding cassette transporters (ABC transporters).

In addition to serving a transport function, glutathione can also reduce Ag^+ to form AgNPs inside the cytosol[9]. Ag^+ reduction may also occur outside the cell[3] by the release of chelating agents, *e.g.*, flavins, carboxylates and phenolics which are primarily intended for the reduction of Fe^{3+} to Fe^{2+}.

As Cu^+ is required throughout the plant, a transport mechanism is necessary for its transport out of the cytosol. For Cu^+, this is primarily accomplished by P-type ATPases (specifically for Cu^+, P_{1b-1} ATPase, also heavy metal ATPases or HMAs). Different types of HMAs are localized differently in cells and tissues, *e.g.*, in rice (*O. sativa*), OsHMA4 is localized in root vacuoles (tonoplast, vacuole membrane) while OsHMA5 is localized in the plasma membrane and is involved in xylem loading of Cu^+.

Since Ag^+ translocation is intrinsically linked to Cu^+ homeostasis, all of the Cu^+ pathways are also utilized by Ag^+. Ag^+ is loaded into the xylem through the same Cu^+ transporters. Once there, it is exposed to citrate which is, in the absence of

silver, used as a chelator of Fe^{3+}. Citrate is able to reduce Ag^+ to form AgNPs in the xylem, enabling the formation and accumulation of NPs in the xylem.

In conclusion, with our current knowledge of Ag^+ uptake, we can expect that both Ag^+ ions and AgNPs are going to be present in plant tissues exposed to $AgNO_3$, with AgNPs of different size being transported to and/or accumulated in different tissues, depending on local transporting and reduction capabilities.

ESI-4: Validation of LA-sp-ICPMS Speciation by Ag L_3-edge μ-XANES

Ag L_3-edge micro-XANES analysis is used to determine the relative ratio between metallic Ag and Ag^+ species in different parts of the sunflower roots. Normalized Ag L_3-edge XANES spectra measured on sunflower root rhizodermis tissue and on cortex/vascular tissues are shown in **Figure S4**, together with the spectra of several Ag reference compounds (metallic Ag and Ag^+ compounds: Ag-nitrate, Ag-acetate, Ag-cyanide, Ag-cysteine).

The energy position of the Ag L_3 absorption edge is correlated with the valence state of Ag atoms in the sample.[10,11] The energy of the Ag L_3-edge in metallic Ag, defined as the first inflection point in the L_3-edge profile, is at 3351.0 eV. The energy position of the Ag L_3-edge in the spectra of Ag^+ species is shifted to higher energies for about 6 to 7 eV compared to the Ag L_3-edge in the metallic Ag. All Ag^+ compounds exhibit a distinct pre-edge resonance from about 3353 to 3355 eV. The pre-edge resonance can be attributed to the transition from 2p to 5s, enhanced by the 5s-4d hybridization of Ag^+ orbitals in different Ag^+ compounds. Its intensity strongly correlates with the strength of the covalent bond between Ag and the ligand.[10]

If the sample contains two or more Ag compounds with different valence states and local structures, the measured Ag L_3-edge XANES spectrum is a linear combination of individual Ag L_3-edge XANES spectra of the constituent Ag compounds. The relative amount of each compound can be determined by the linear combination fitting (LCF) of XANES spectra.[12] For both sunflower root spectra the best fit is obtained with a linear combination of three components: Ag metal, Ag-cyanide and Ag-cysteine (**Figures S5 and S6**). The results of LCF analysis show that sunflower root rhizodermis tissue contains 72 % of metallic Ag and 28 % of Ag^+ species, while in the cortex/vascular tissues the metallic Ag content is only 15% with the rest attributed to Ag^+ species.

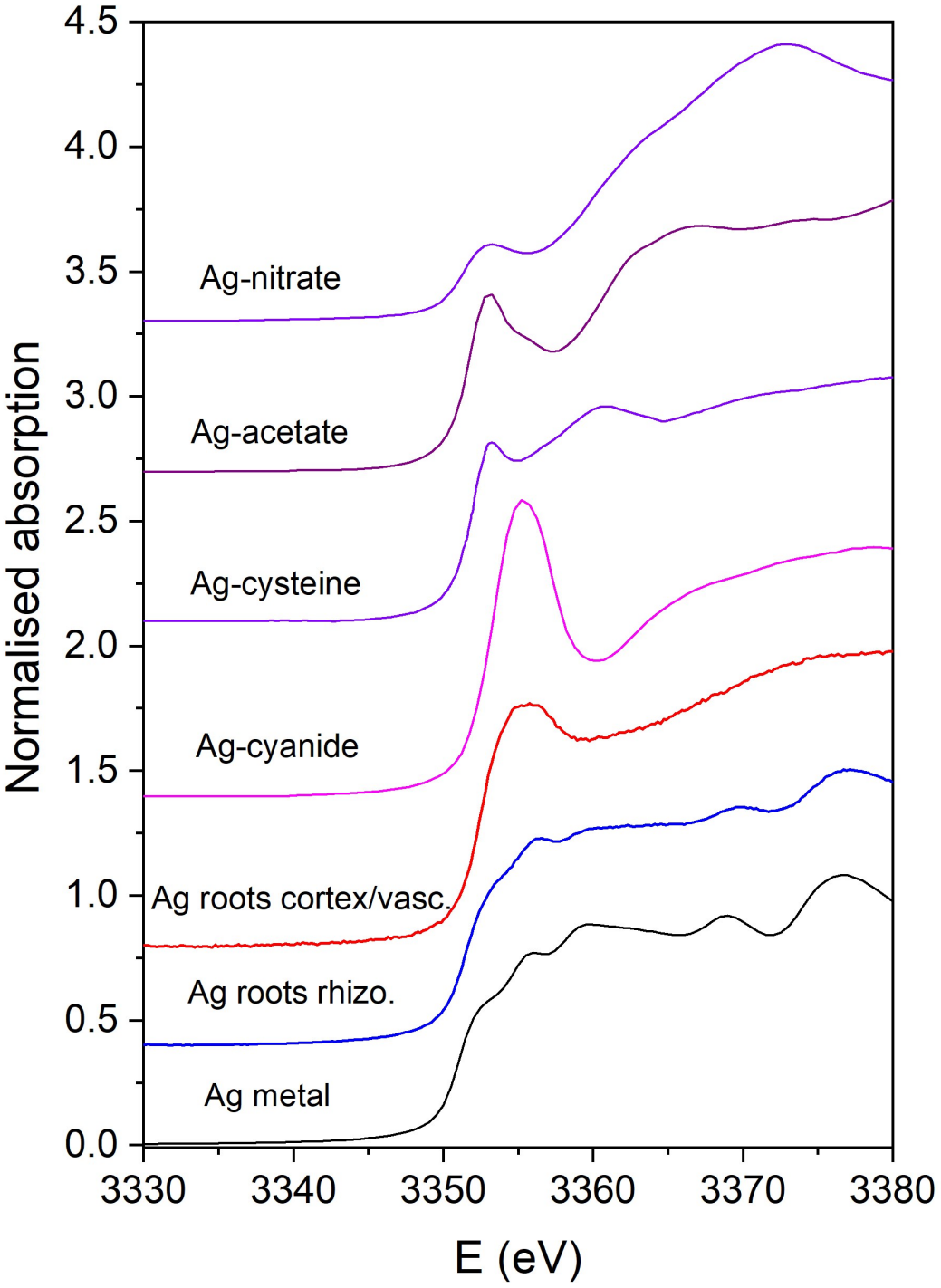

Figure S4. Normalized Ag L_3-edge XANES spectra measured in sunflower root rhizodermis tissue and cortex/vascular tissues. Ag L_3-edge XANES spectra of reference Ag compounds (metallic Ag and Ag^+ compounds: Ag-nitrate, Ag-acetate, Ag-cyanide and Ag-cysteine) are shown for comparison.

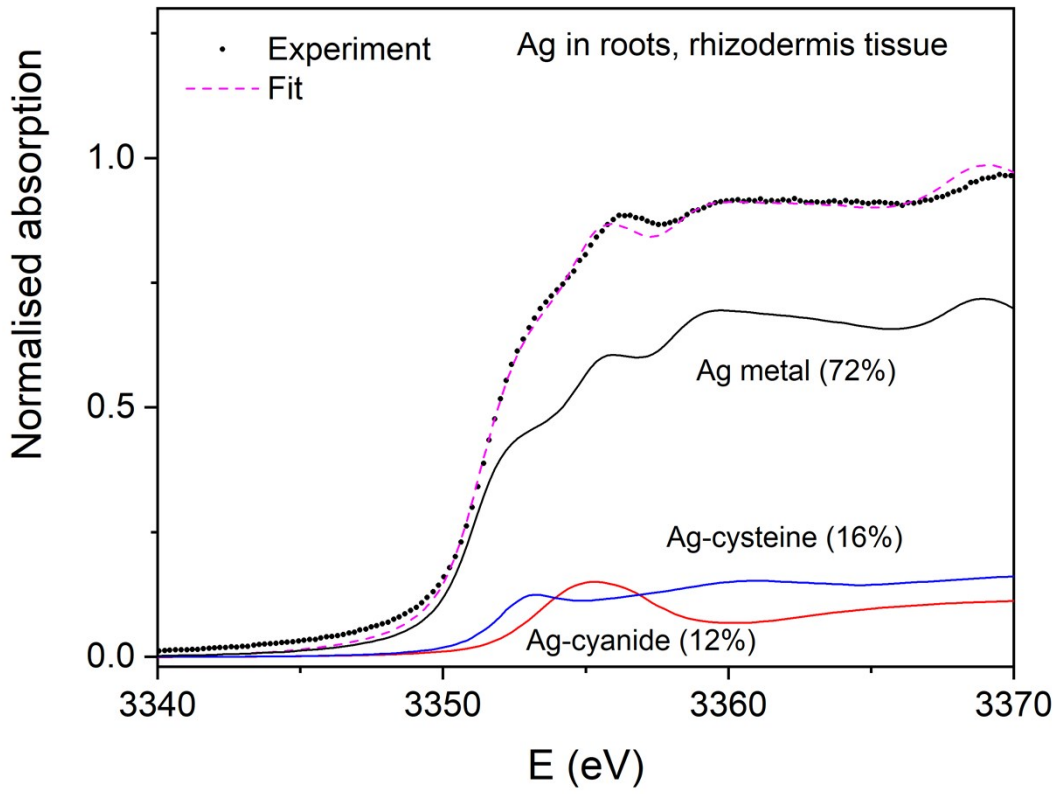

Figure S5. Ag L_3-edge XANES spectrum measured in sunflower root rhizodermis tissue. Dots: experiment; dashed magenta line: best fit linear combination of the three reference XANES profiles (Ag metal (72 %), Ag-cyanide (12 %) and Ag-cysteine (16 %)).

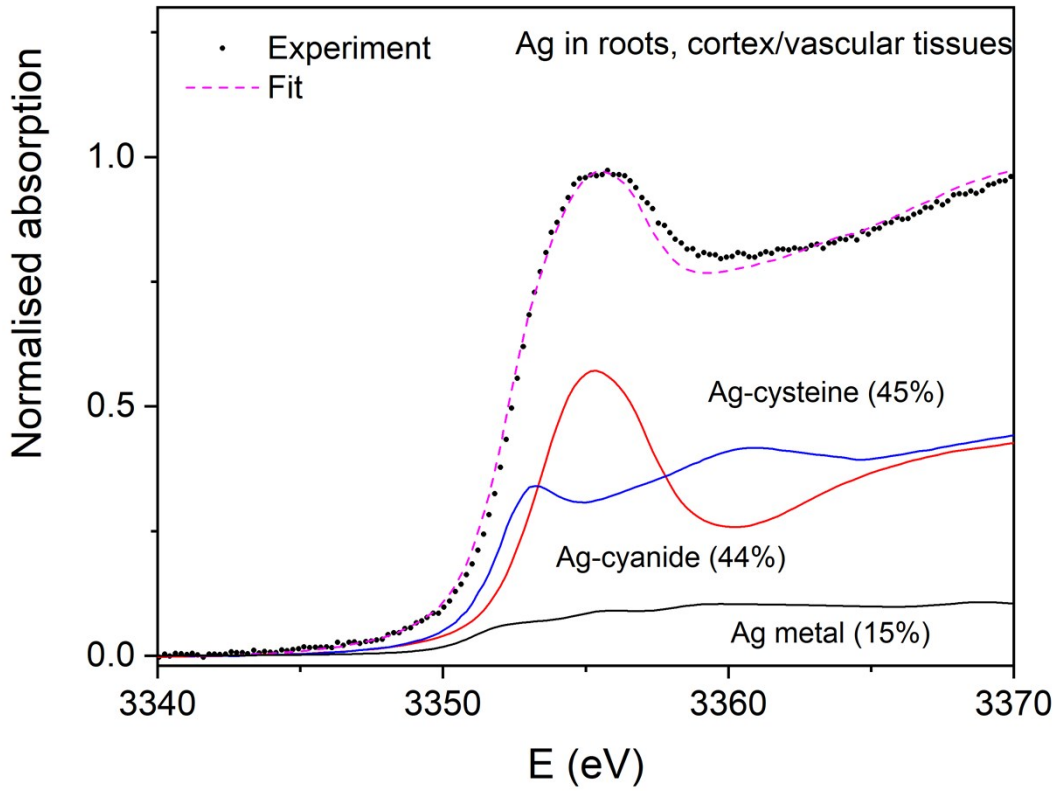

Figure S6. Ag L_3-edge XANES spectrum measured in sunflower cortex/vascular tissues. Dots: experiment; dashed magenta line: best fit linear combination of the three reference XANES profiles (Ag metal (15 %), Ag-cyanide (44 %) and Ag-cysteine (45 %)).

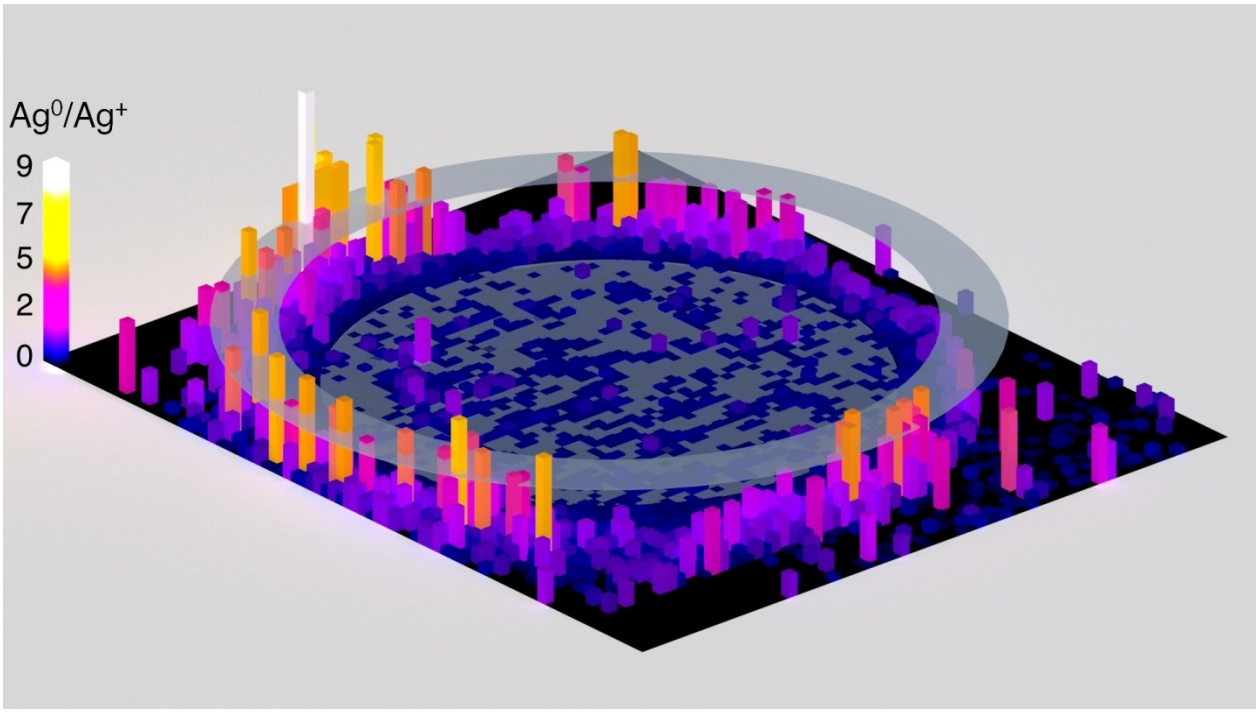

Figure S7. The AgNP : Ag^+ mass ratio per pixel as constructed from LA-sp-ICPMS data (pixelated map) and the average Ag^0 : Ag^+ ratio in the rhizodermis (grey ring) and the cortex and vascular tissues (grey disk) as obtained by μ-XANES (probed on several locations), associated with a sunflower root cross-section exposed to 40 μg g^{-1} Ag (as $AgNO_3$) in hydroponics.

References

1 D. Mozhayeva and C. Engelhard, *J. Anal. At. Spectrom.*, , DOI:10.1039/c9ja00206e.
2 T. O'Haver, (https://Www.Mathworks.Com/Matlabcentral/Fileexchange/23611-Peakfit-m), MATLAB Central File Exchange. MATLAB Central File Exchange 2020.
3 M. González-Guerrero, V. Escudero, Á. Saéz and M. Tejada-Jiménez, *Front. Plant Sci.*, 2016, **7**, 1–21.
4 E. Andresen, E. Peiter and H. Küpper, *J. Exp. Bot.*, 2018, **69**, 909–954.
5 P. Zandi, J. Yang, K. Możdżeń and B. Barabasz-Krasny, *Adv. Agron.*, 2020, **160**, 249–293.
6 W. Maret and A. Wedd, Eds., *Binding, Transport and Storage of Metal Ions in Biological Cells*, Royal Society of Chemistry, Cambridge, 2014.
7 E. B. Maryon, S. A. Molloy and J. H. Kaplan, *Am. J. Physiol. - Cell Physiol.*, 2013, **304**, 768–779.
8 M. Hasanuzzaman, K. Nahar, T. I. Anee and M. Fujita, *Physiol. Mol. Biol. Plants*, 2017, **23**, 249–268.
9 M. Bagherzadeh Homaee and A. A. Ehsanpour, *Hortic. Environ. Biotechnol.*, 2016, **57**, 544–553.
10 T. Miyamoto, H. Niimi, Y. Kitajima, T. Naito and K. Asakura, *J. Phys. Chem. A*, 2010, **114**, 4093–4098.
11 C. Larue, H. Castillo-Michel, S. Sobanska, L. Cécillon, S. Bureau, V. Barthès, L. Ouerdane, M. Carrière and G. Sarret, *J. Hazard. Mater.*, 2014, **264**, 98–106.
12 B. Ravel and M. Newville, *J. Synchrotron Radiat.*, 2005, **12**, 537–541.